Nonisothermal Crystallization, Melting Behavior, and Morphology of Polypropylene/Metallocene-Catalyzed Polyethylene Blends

Jungang Gao, Dong Wang, Maoshang Yu, Zihua Yao

College of Chemistry and Environmental Science, Hebei University, Baoding 071002, People's Republic of China

Received 25 July 2003; accepted 12 January 2004
DOI 10.1002/app.20505
Published online in Wiley InterScience (www.interscience.wiley.com).

ABSTRACT: The nonisothermal crystallization, melting behavior, and morphology of blends of polypropylene (PP) and a metallocene-catalyzed polyethylene (mPE) elastomer were studied with differential scanning calorimetry, scanning electron microscopy, polarized optical microscopy, and X-ray diffraction. The results showed that PP and mPE were partially miscible and could form some cocrystallization, although the extent was very small. A modified Avrami analysis and the Mo method were used to analyze the nonisothermal crystallization kinetics of the blends. The values of the Avrami exponent indicated that the crystallization nucleation of the blends was homogeneous, the growth of the spherulites was three-dimensional, and the crystallization mechanism of PP was not affected by mPE. The crystallization activation energy was estimated with the Kissinger method. Interesting results were obtained with the modified Avrami analysis and Mo and Kissinger methods, and the conclusions were in good agreement. The addition of less mPE increased the overall crystallization rate of PP. The relationship between the composition and morphology of the blends was examined. © 2004 Wiley Periodicals, Inc. J Appl Polym Sci 93: 1203–1210, 2004

Key words: crystallization; morphology; polyethylene (PE); poly(propylene) (PP)

INTRODUCTION

Polypropylene (PP) is one of the most widely used polyolefin polymers, but its applications in some fields are limited because of its low fracture toughness at low temperatures and its high notch sensitivity at room temperature. The compounding of PP with a dispersed elastomeric phase [e.g., ethylene–propylene–diene copolymer (EPDM)] is widely practiced[1–5] because the rubber can increase the overall toughness of the PP matrix.[6] However, the addition of elastomers often has negative effects on some properties of PP, such as the stiffness and hardness.[7]

The development of metallocene catalysts has led to numerous new polyolefinic materials, among which polyolefin elastomers are extremely attractive to both the rubber and plastics industries. Metallocene-catalyzed polyethylene (mPE) elastomers polymerized with octene as a comonomer possess a very homogeneous copolymer distribution and a narrow molecular mass distribution.[8] In comparison with conventional EPDM, mPE elastomers can impart higher impact strength and better dynamic properties as a modifier of PP.[9,10] Moreover, mPE is granular, so blending it with PP (e.g., during extrusion and injection molding) is convenient.

The physical properties of semicrystalline polymeric materials strongly depend on their crystallization and microstructures, and so investigations of the crystallization behavior and morphology of polymer blends are significant both theoretically and practically. In particular, crystallization behavior during nonisothermal crystallization is increasingly important technologically because these conditions are the closest to practical industrial conditions. Therefore, investigating the crystallization behavior and morphology to optimize the blend composition and processes and understand the properties of the processed products is highly desirable. However, such detailed investigations have not been reported until now.

In this study, the nonisothermal crystallization and melting behavior of PP/mPE blends were investigated to examine (1) the phase behavior and possibility of cocrystallization in PP/mPE blends, (2) the validity of the modified Avrami analysis and Mo method for the nonisothermal crystallization of PP in mPE blends, and (3) the effect of mPE on the PP crystallization mechanism. The morphology of the blends was also studied to determine the effect of mPE on the microstructures of the blends.

Correspondence to: J. Gao (gaojg@mail.hbu.edu.cn).
Contract grant sponsor: Natural Science Foundation (Hebei Province, China); contract grant number: 201068.
Contract grant sponsor: Educational Science Foundation (Hebei Province, China); contract grant number: 2000105.

EXPERIMENTAL

Materials and sample preparation

The PP [type T30S, d = 0.901 g/cm^3, melt-flow index (230°C/2.16 kg) = 3.88 g/10 min, tacticity = 96.6%] used in this study was a commercial polymer supplied by Daqing Petrochemical Co. (China). mPE [type 0201C-8, d = 0.895 g/cm^3, melt-flow index (230°C/2.16 kg) = 3.12 g/10 min] was obtained from Qatar Petrochemical Co.

Blend samples were prepared via melt blending on a two-roll mill at 180°C for 10 min. The PP/mPE ratios (w/w) were 100/0, 90/10, 80/20, 70/30, 60/40, 40/60, 20/80, and 0/100. The melt of the blends was compressed in an electric-heat press for 5 min at 16 MPa and 180°C and was cold-pressed for 10 min at 5 MPa; 4-mm-thick sheets were produced.

Thermal analysis

A PerkinElmer DSC-7 apparatus was used to investigate the melting and nonisothermal crystallization behavior of the blends. All the operations were carried out under a nitrogen environment. The temperature and melting enthalpy were calibrated with standard indium. The sample weight was about 7.4 mg.

For the melting behavior, samples were heated from room temperature to 210°C at a rate of 20°C/min. To erase the influence of the thermal history, a second run was carried out after the melted samples were cooled to 50°C. As for nonisothermal crystallization, samples were heated from room temperature to 210°C and held at this temperature for 5 min; they were then cooled down to 50°C at various constant cooling rates (2.5, 5, 10, and 20°C/min).

Morphology analysis

Scanning electron microscopy (SEM) micrographs were taken on a KYKY model 1000B microscope with the method of Campbell and White.[11] Fracture surfaces taken from impact fracture sections were examined.

Polarized optical microscopy (POM) micrographs were obtained with an XPT-7 polarized optical microscope equipped with an Olympus camera. A compression-molded film was sandwiched between a microscope slide and a cover glass, and then the sample was heated from room temperature to 210°C, kept at this temperature for 5 min to allow complete melting, and then cooled to 140°C at a cooling rate of 2°C/min for isothermal crystallization for 1 h.

X-ray diffraction (XRD) patterns were recorded on a Y-2000 diffractometer with Cu Kα radiation. The data were collected in the 2θ range of 5–32° with λ = 1.54178Å and at a scanning rate of 0.06° s^{-1}. The blend specimens for XRD measurements were obtained in sheet form and were prepared in an electric-heat press.

TABLE I
Melting Peak Temperatures and Crystallinity of PP/mPE Blends

Sample (PP/mPE)	T_{mp1} (°C)	T_{mp2} (°C)	ΔH_{m1} (J/g)	ΔH_{m2} (J/g)	X_m (%)	X_x (%)
100/0		162.2		84.09	44.80	40.36
80/20	96.6	161.6	5.88	60.75	34.47	35.26
60/40	96.1	162.1	17.61	41.7	28.53	30.94
40/60	94.8	159.8	30.52	26.84	25.24	24.38
20/80	92.0	158.3	45.72	12.35	22.97	21.83
0/100	95.8		59.21		21.22	18.37

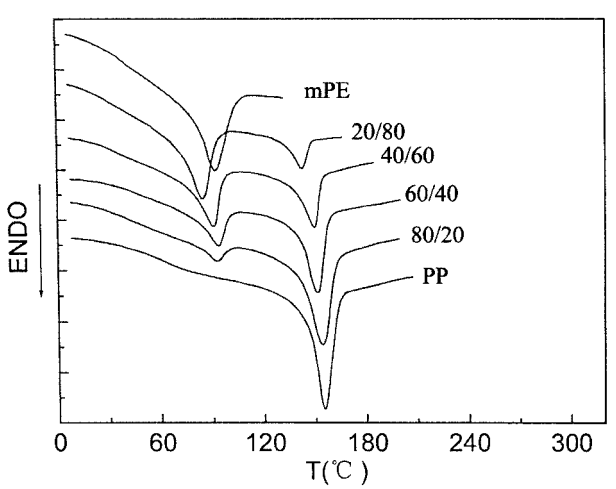

Figure 1 DSC melting curves of PP/mPE blends (heating rate = 20°C/min).

RESULTS AND DISCUSSION

Melting and crystallization behavior of the PP/mPE blends

Figure 1 shows differential scanning calorimetry (DSC) melting curves of the pure polymers and their blends. The melting peak temperature of PP (T_{mp2}) decreases as the mPE content increases (see Table I); however, the melting peak temperature of mPE (T_{mp1}) increases with increasing PP content. This indicates that there is some interaction between PP and mPE, which can be attributed to the partial miscibility of molecules of PP and mPE. T_{mp2} for the blends is around 160°C. This indicates that PP, both in the pure state and in the blends, exhibits only the α-crystal form because the melting temperature of the α-crystal form is in the range of 160–176°C;[12,13] this is consistent with the XRD data, which are discussed later. The melting crystallinity (X_m) of the PP/mPE blends decreases with the mPE content (Table I), and this indicates that the mPE component reduces the total crystallinity (X_{total}) of the blends.

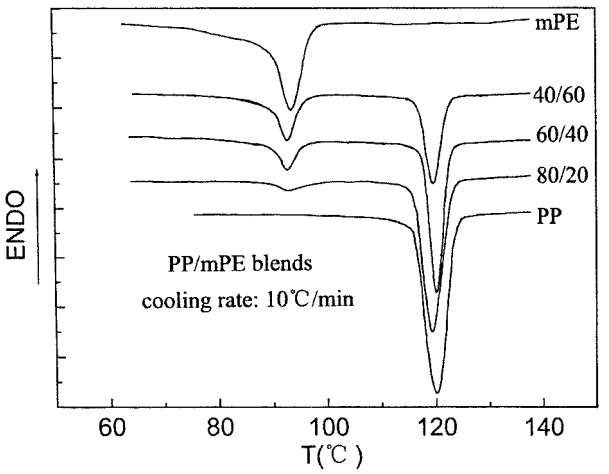

Figure 2 DSC nonisothermal crystallization curves of PP/mPE blends (cooling rate = 10°C/min).

For the pure PP, pure mPE, and their blends, nonisothermal crystallization was performed from the molten state with DSC at various cooling rates (2.5–20°C/min). Figure 2 shows the crystallization exotherms for some PP/mPE blends and pure PP and pure mPE (cooling rate = 10°C/min). All the DSC traces of the blends show two crystallization peaks, which indicate that these blend systems have two crystallizable components. The crystallization of PP occurs much earlier than that of mPE upon cooling. Whether or not the PP crystallization is affected by the mPE phase is one of the main questions of this work.

As an example, Figure 3 shows typical crystallization exotherms for PP in an 80:20 PP/mPE blend at various cooling rates. The crystallization peak temperature (T_p) for the pure polymers and their blends is clearly shifted to lower temperatures as the cooling rate increases (see Table II). The reduction of T_p at a faster cooling rate is due to the crystallization rate being slower than the experimental cooling rate.[14] At a slower cooling rate, PP molecules have enough time to form a more complete crystal and, therefore, reach a higher T_p.

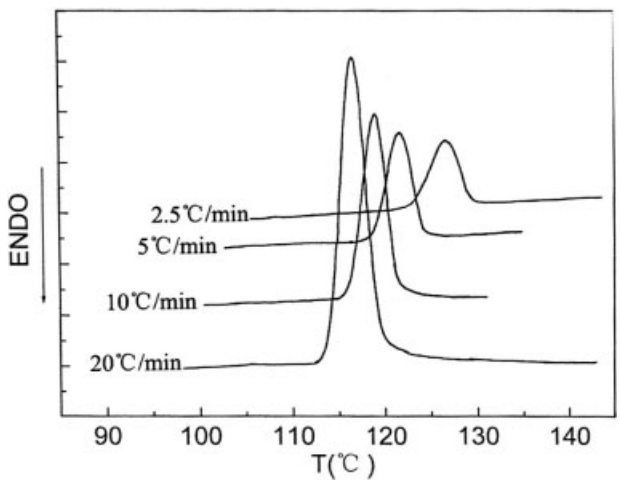

Figure 3 DSC nonisothermal crystallization curves of PP in 80:20 PP/mPE blends at various cooling rates.

TABLE II
Nonisothermal Crystallization Parameters of PP/mPE Blends at Different Cooling Rates

Sample (mPE %)	D (°C/min)	n	k' ($\min^{-n}$)	$t_{1/2}$ (min)	T_p (°C)	X_{total} (%)
	2.5	4.36	0.03	5.83	125.8	47.04
	5.0	4.19	0.35	3.23	122.9	45.10
0	10	4.18	0.76	1.76	120.0	43.93
	20	3.90	1.02	0.91	117.5	40.27
	2.5	4.48	0.04	5.37	125.8	41.38
	5.0	4.10	0.39	2.92	121.5	38.70
20	10	4.12	0.83	1.47	119.0	37.36
	20	4.03	1.03	0.82	116.1	34.11
	2.5	4.50	0.04	5.14	126.5	34.57
	5.0	4.36	0.38	2.78	123.9	32.22
40	10	4.34	0.93	1.28	120.0	30.01
	20	4.10	1.05	0.69	116.7	26.24

For all the samples, X_{total} is defined as follows:

$$X_{total} = \left(\frac{\Delta H_{f1}}{\Delta H_{f1}^0} + \frac{\Delta H_{f2}}{\Delta H_{f2}^0}\right) \quad (1)$$

where ΔH_{f1} and ΔH_{f1}^0 are the melting enthalpies of a PP sample and 100% crystallized PP, respectively (ΔH_{f1}^0 = 187.7 J/g),[15] and ΔH_{f2} and ΔH_{f2}^0 are the melting enthalpies of an mPE sample and 100% crystallized PE, respectively (ΔH_{f2}^0 = 279 J/g).[16] As shown in Table II, X_{total} decreases as the cooling rate increases. Meanwhile, at the same cooling rate, X_{total} also changes with the blend composition, and this indicates that X_{total} of the blends decreases with the addition of mPE. That agrees with the X_m values found in DSC heating runs. This may be explained as follows: PP and mPE are partially miscible, and so the crystallization ability of PP is disrupted by mPE in the molten state. These results show that increasing both the cooling rate and the mPE content can reduce the crystallinity.

Nonisothermal crystallization kinetics

Several analytical methods have been developed to describe the nonisothermal crystallization kinetics of polymers: (1) the modified Avrami analysis;[17–19] (2) the Ozawa analysis;[20,21] (3) the Ziabicki analysis;[22,23] and (4) others,[24–27] such as the Mo analysis. In this article, the modified Avrami analysis and Mo analysis are used to describe the nonisothermal crystallization kinetics of PP/mPE blends, and a contrastive study has been undertaken.

The Avrami equation[19,28,29] has been widely used to describe the isothermal crystallization kinetics of polymers:

$$1 - X_t = \exp(-kt^n) \tag{2}$$

where X_t is the relative crystallinity, k is the growth rate constant, and n is the Avrami exponent. Here, the value of n depends on the nucleation mechanism and growth dimension, and parameter k is a function of the nucleation and growth rate. X_t, as a function of the crystallization time, is defined as follows:

$$X_t = \frac{\int_{t_0}^{t} (dH_c/dT)\, dT}{\int_{t_0}^{t_\infty} (dH_c/dT)\, dT} \tag{3}$$

where dH_c/dT is the rate of heat evolution and t_0 and t_∞ are the times at which crystallization starts and ends, respectively.

The Avrami equation can be modified to describe nonisothermal crystallization.[17,18,30,31] For nonisothermal crystallization at a chosen cooling rate, X_t is a function of the crystallization temperature (T). That is, eq. (3) can be rewritten as follows:

$$X_t = \frac{\int_{T_0}^{T} (dH_c/dT)\, dT}{\int_{T_0}^{T_\infty} (dH_c/dT)\, dT} \tag{4}$$

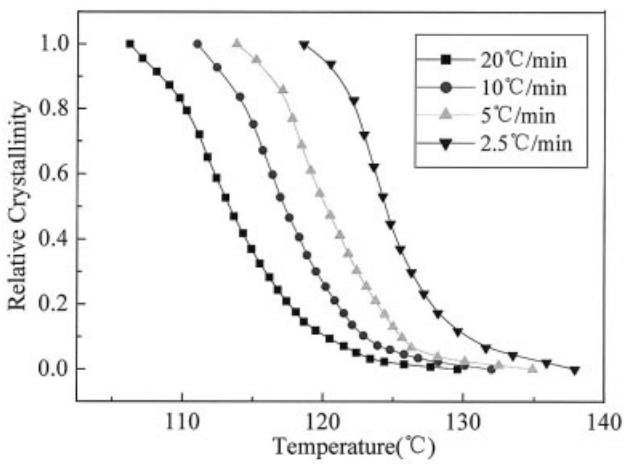

Figure 4 Relative crystallinity versus the crystallization temperature for PP in 80:20 PP/mPE blends for nonisothermal crystallization at various cooling rates.

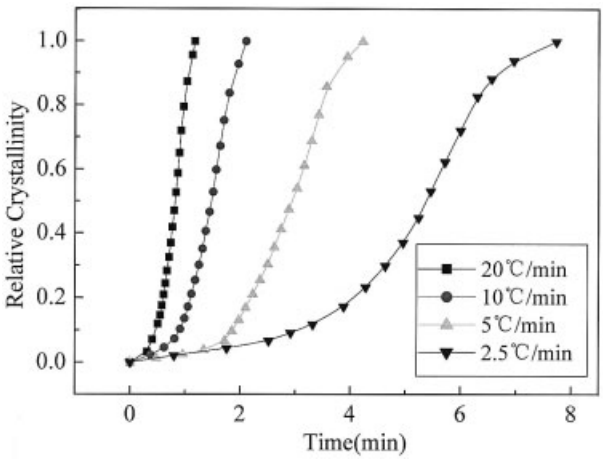

Figure 5 Relative crystallinity versus the crystallization time for PP in 80:20 PP/mPE blends for nonisothermal crystallization at various cooling rates.

where T_0 and T_∞ represent the onset and end temperatures of crystallization, respectively.

As an example, Figure 4 shows the X_t values of PP in PP/20% mPE blends at various cooling rates. All the curves in Figure 4 show a reversed sigmoidal shape, indicating a fast primary process during the initial stages and slower secondary process during the later stages. The plot of X_t versus T shifts to a low-temperature region as the cooling rate increases, indicating that the crystallization is enhanced as the temperature decreases. This is due to the strong temperature dependence of the nucleation and the growth parameters.[32] After the maximum in the heat-flow curves has passed, a large fraction of crystallinity develops by slower, secondary kinetic processes. The slower cooling rate provides more fluidity and diffusivity for the molecules because of the lower viscosity and more time for the perfection of crystallization, thus inducing much higher crystallinity at a higher temperature than for the samples cooled at fast cooling rates, as shown in Figure 4.

T can be converted into crystallization time t with the following equation:[23,30]

$$t = \frac{T_0 - T}{D} \tag{5}$$

where D is the cooling rate (°C/min). With eq. (5), the temperature axis in Figure 4 can be transformed into a timescale, as shown in Figure 5. The sigmoidal shape of the curves suggests that the extended Avrami analysis is applicable to the nonisothermal crystallization of PP/mPE blends. Meanwhile, the crystallization half-time ($t_{1/2}$) can be calculated directly from a plot of X_t versus time,[19,33] as shown in Table II.

Equation (2) can be rewritten in a double-logarithm form:

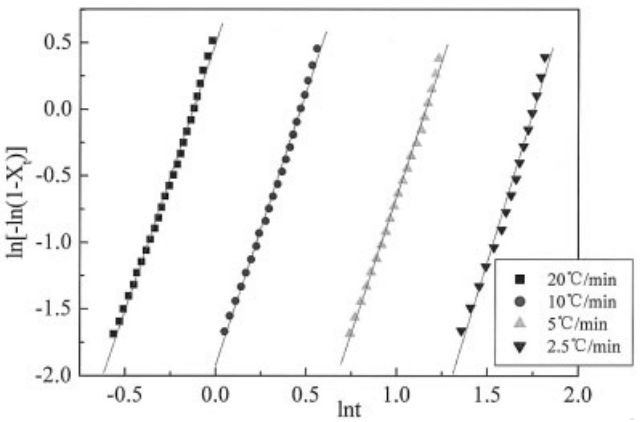

Figure 6 Avrami plot for PP in 80:20 PP/mPE blends for nonisothermal crystallization at various cooling rates.

$$\ln[-\ln(1 - X_t)] = \ln k + n \ln t \quad (6)$$

The Avrami parameters can be estimated from a plot of $\ln[-\ln(1 - X_t)]$ versus $\ln t$. Here, the crystallization rate of nonisothermal crystallization depends on the cooling rate. Thus, the crystallization rate constant k should be corrected adequately. At a constant cooling rate, k can be corrected as follows:[30] $\ln k' = \ln k/D$.

Figure 6 shows a plot of $\ln[-\ln(1 - X_t)]$ versus $\ln t$ for the nonisothermal crystallization of PP/20% mPE blends. All the lines in Figure 6 are parallel, shifting to lower times as the cooling rate increases. This implies that the nucleation mechanism and crystal growth geometries are similar, although the cooling rates are different. The Avrami parameters have been estimated from the plot of $\ln[-\ln(1 - X_t)]$ versus $\ln t$, and the values are listed in Table II. Regardless of the cooling rates, n for pure PP is 3.90–4.36, in good agreement with literature data under nonisothermal conditions, indicating homogeneous nucleation and three-dimensional growth of spherulites.[34] The Avrami exponents for the PP/mPE blends are 4.03–4.50, regardless of the blend composition and cooling rates, suggesting that the effects of mPE on nucleation and the forms of growth in PP crystallization are insignificant.

However, the crystallization rate is dependent on the blend composition and cooling rates. On the one hand, for pure PP, k' increases with the cooling rate, whereas $t_{1/2}$ decreases with an increasing cooling rate (see Table II). Similar trends in both k' and $t_{1/2}$ have been observed for PP/20% mPE and PP/40% mPE blends. On the other hand, both k' and $t_{1/2}$ are also influenced by the addition of mPE; that is, at the same cooling rate, k' slightly increases as the mPE content increases, and $t_{1/2}$ is adversely affected. Thus, the crystallization rate is accelerated with the addition of mPE to PP, and this is due to the molecular mobility in the blends increasing because the mPE elastomer has a lower crystallinity and melting temperature. Meanwhile, the tacticity and flexibility of the molecular chain of mPE are high, the activity of the molecule is also high, and so is the crystallization rate. Thus, at a higher temperature, the addition of mPE increases the crystallization rate of the blends.

For comparison, a new simple method proposed by Mo et al.[24] can be used as follows:

$$\ln D = \ln F(T) - \alpha \ln t \quad (7)$$

where $F(T) = [K(T)/k]^{1/m}$ refers to the cooling rate value, which must be chosen within the unit of the crystallization time when the measured system amounts to a certain value of X_t. The $F(T)$ value has a definite physical and practical meaning; that is, at a certain value of X_t, a high value of $F(T)$ is needed to reach this X_t value in a unit of time. $F(T)$ reflects the difficulty of the crystallization process. a is the ratio of Avrami exponent n to Ozawa exponent m ($a = n/m$). According to eq. (7), $F(T)$ and a can be determined from the slope and intercept of a double-logarithm plot of the cooling rate versus time. Figure 7 presents the results for PP/20% mPE blends at different X_t values of 20, 40, 60, and 80%, respectively. The values of $F(T)$ and a for all the samples are listed in Table III. The $F(T)$ values increase with X_t for the same blend. However, at the same X_t value, the values of $F(T)$ of PP are higher than those of PP/mPE blends, and this implies faster crystallization for the PP/mPE blends than for PP. This conclusion agrees with the results obtained from the modified Avrami analysis. The values of a are almost constant for a given composition and different X_t values, and this indicates that the method is successful in describing the nonisothermal crystallization process of PP/mPE blends.

For nonisothermal crystallization, the crystallization activation energy (E_a) can be estimated from the variation of T_p with D by the Kissinger approach:[35]

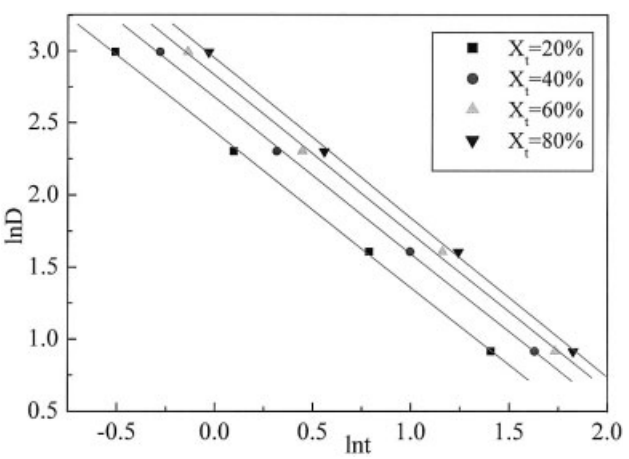

Figure 7 Mo plot for PP in 80:20 PP/mPE blends for nonisothermal crystallization at different values of X_t.

TABLE III
Nonisothermal Crystallization Parameters of PP/mPE Blends at Different Relative Crystallinities

Sample (mPE %)	X_t (%)	$F(t)$	a	E_a (kJ/mol)
0	20	12.11	1.041	329.32
	40	15.33	1.069	
	60	17.96	1.068	
	80	20.25	1.072	
20	20	11.41	1.076	286.03
	40	14.50	1.081	
	60	16.95	1.093	
	80	19.09	1.107	
40	20	10.02	1.078	274.62
	40	13.99	1.088	
	60	16.92	1.110	
	80	18.70	1.113	

$$\frac{d[\ln(D/T_p^2)]}{d(1/T_p)} = -\frac{E_a}{R} \tag{8}$$

where R is the universal gas constant.

A Kissinger plot, that is, a plot of $\ln(D/T_p{}^2)$ versus $1/T_p$, for PP/mPE blends is shown in Figure 8. E_a has been estimated to be 329.32 kJ/mol for pure PP, 286.03 kJ/mol for PP/20% mPE blends, and 274.62 kJ/mol for PP/40% mPE blends (see Table III). E_a of pure PP is higher than that of the PP/mPE blends. As for the kinetics, the activation energy can be correlated to the crystallization rate. As described earlier in this study, the crystallization rate decreases in the following order: PP/40% mPE blends > PP/20% mPE blends > pure PP (see Table II). The crystallization rate obtained by the Mo method follows the same decreasing order (see Table III). That is, a lower activation energy of crystallization drives a more rapid crystallization rate. This may result from the fact that the PP polymer chains in the blends are packed more easily than the pure PP chains; this can be attributed to the diluent effect of mPE.

Morphology analysis

It is well known that the properties of materials greatly depend on their morphological structure. For polymer blends or composites, the dispersion of the components is extremely important. A series of SEM micrographs of fracture surfaces obtained during the notch testing of PP/mPE blends are shown in Figure 9, and they clearly demonstrate the uniform dispersion of the mPE components in PP. Pure PP [Fig. 9(A)] has a relatively smooth surface and exhibits a brittle fracture behavior. A coarser appearance can be observed on the fractured surfaces of the blends containing 10% mPE [Fig. 9(B)], but it can be still characterized as a semibrittle fracture, with only a little plastic deformation. As the content of mPE increases [Fig. 9(C,D)], these fracture surfaces are accompanied by extensive plastic deformation, the mPE phases are homogeneously dispersed in the PP matrix, and a sea-island structure forms. mPE forms a dispersed phase, and the dimensions depend on the blend composition. With 10% mPE, the dispersed phase is rather small (0.2–0.6μm) and is not homogeneous. With 30% mPE, the dispersed phase is approximately 3–5 times larger (1.0–2.0μm) than that with 10% mPE.

Figure 10 shows POM micrographs of PP/mPE blends isothermally crystallized at 140°C for 1 h. As shown in Figure 10(A), pure PP has a well-defined and large spherulite morphology; the spherulites grow and impinge on one another to form particular polygonal spherulites with clear boundaries. With the addition of 10% mPE, the PP spherulite decreases in size, but a right-angle intersection is still evident and clear [see Fig. 10(B)]. When the mPE content increases to 20 [Fig. 10(C)] and 30% [Fig. 10(D)], the spherulite size promptly decreases, and with less perfection, the right-angle intersection disappears, the spherulite boundaries become more diffuse, and interspherulitic interaction increases. Overall, the addition of mPE greatly affects the spherulite size and morphology of PP. The spherulite size promptly decreases; this is due to the cocrystallization and crystallizability of PP being disrupted by the higher concentration of mPE. The PP molecular chains are more difficult to pack in an ordered manner than those of pure PP; this causes a large number of spherulites to grow in a limited space. Therefore, perfect spherulites cannot form at a higher concentration of mPE. In addition, the large number of nucleus centers causes more crystalline defects and leads to a low crystallinity.

Figure 11 shows XRD patterns for PP, mPE, and their blends. Strong diffraction peaks are located at 2θ diffraction angles of 14.02, 16.82, 18.52, and 21.78° (a doublet), the former three peaks of which correspond

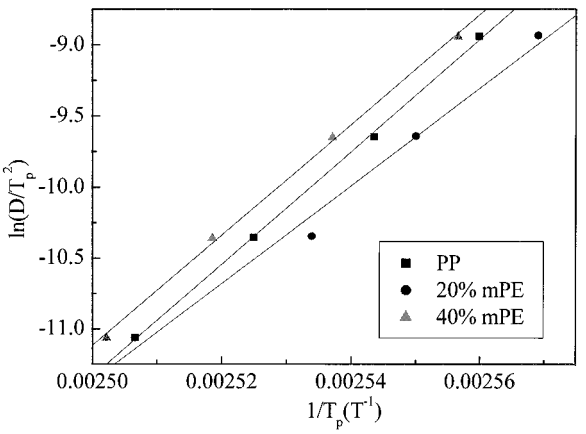

Figure 8 Kissinger plot of $\ln(D/T_p{}^2)$ versus $1/T_p$ for PP/mPE blends for nonisothermal crystallization at different mPE contents.

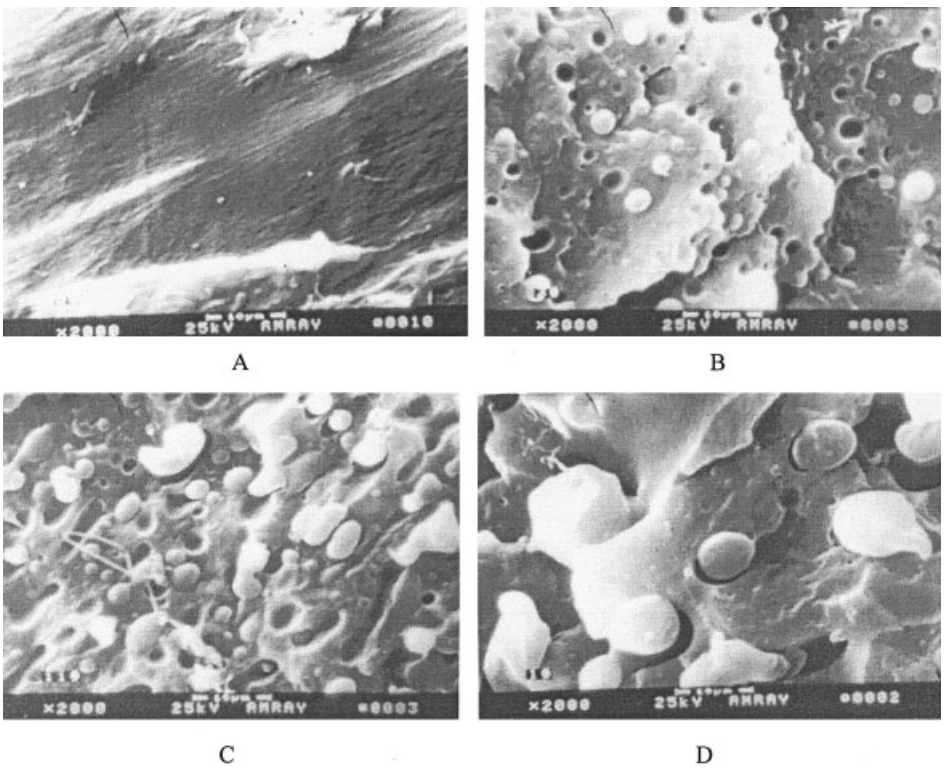

Figure 9 SEM micrographs of PP/mPE blends: (A) pure PP, (B) 10% mPE, (C) 20% mPE, and (D) 30% mPE.

to (110), (040), and (130) planes, respectively, and are characteristic of the typical α-form monoclinic structure of PP.[36,37] Figure 11(A,E) shows that PP prepared from the melt produces only the α-crystal form. mPE

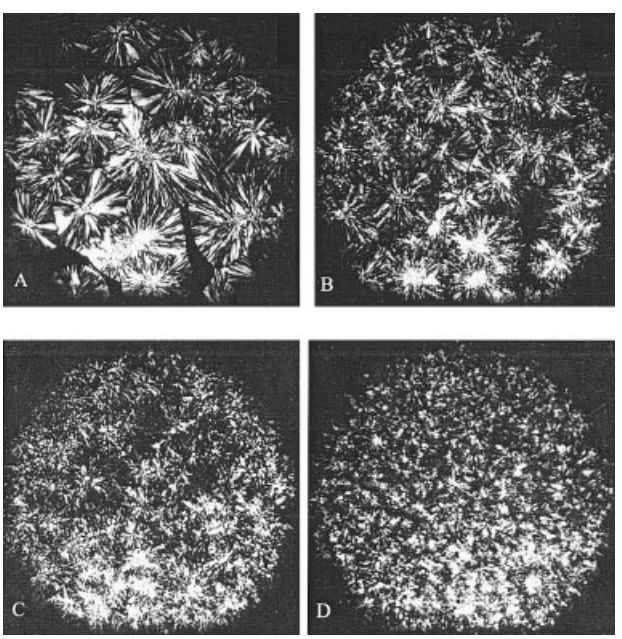

Figure 10 POM micrographs of PP/mPE blends: (A) pure PP (100×), (B) 10% mPE (100×), (C) 20% mPE (100×), and (D) 30% mPE (100×).

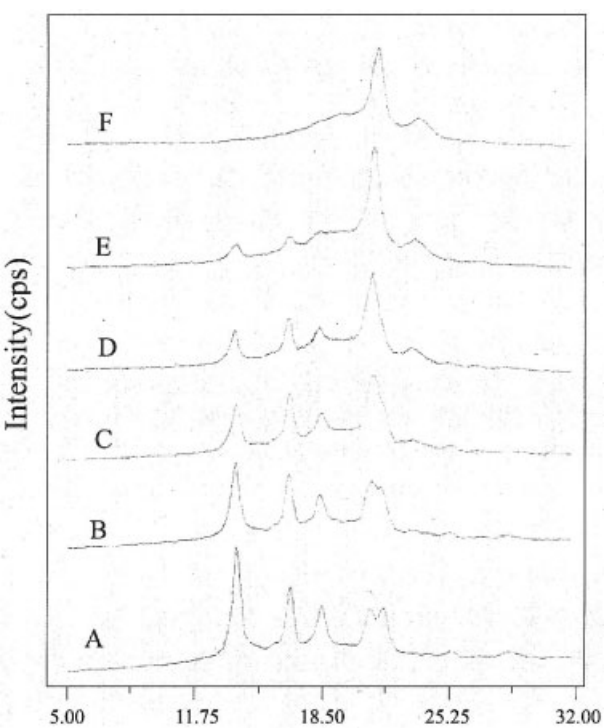

Figure 11 XRD patterns of PP/mPE blends: (A) pure PP, (B) 20% mPE, (C) 40% mPE, (D) 60% mPE, (E) 80% mPE, and (F) pure mPE.

does not clearly show any of these crystal forms, and in the binary blends mPE exhibits only a crystal form in Figure 11(B–E) from a diffraction peak appearing at $2\theta = 21.73°$. For the blends, the intensity of the PP peak decreases as the mPE content increases. The broadened background scattering area of the curves suggests the presence of an amorphous structure. The crystallinity can be estimated with the following formula:[38]

$$\text{Crystallinity (\%)} = \frac{S_c}{S_c + S_a} \times 100 \qquad (9)$$

where S_c is the area of crystallization and S_a is the background area. As shown in Table I, the XRD crystallinity (X_x) decreases with the blend composition, in good agreement with the nonisothermal crystallization process.

CONCLUSIONS

This study of the melting and nonisothermal crystallization behavior of PP/mPE blends has shown that PP and mPE are miscible to a very small extent. The crystallinity of the blends decreases with increasing mPE content.

The values of the Avrami exponent are 3.90–4.50, regardless of the cooling rates and blend composition, and this indicates that the crystallization nucleation is homogeneous and that the nucleation and growth mechanism of PP is not affected by the addition of mPE.

The crystallization rate of the blends is influenced by the composition and the cooling rate. At the same cooling rate, the crystallization rate increases with increasing mPE content. The crystallization activation energy is affected by the composition and is reduced by the addition of mPE, in agreement with the modified Avrami and Mo analysis.

The SEM observations indicate that the mPE phase uniformly disperses in the PP matrix, and the dimensions of the dispersed phase increase with the blend composition. The POM results lead us to the conclusion that the spherulite morphology and size are greatly affected by mPE, and the addition of mPE results in a prompt reduction of the spherulite size. The XRD results show changes in the intensities of the peak of PP and demonstrate that only an α-form monoclinic structure is formed.

References

1. Karger-Kocsis, J.; Kalló, A.; Kuleznev, V. N. Polymer 1984, 25, 279.
2. Coppola, F.; Greco, R.; Martuscelli, E.; Kammer, H. W. Polymer 1987, 28, 47.
3. Tam, W. Y.; Cheung, T.; Li, R. K. Y. Polym Test 1996, 15, 452.
4. Van der Wal, A.; Mulder, J. J.; Oderkerk, J.; Gaymans, R. J. Polymer 1998, 39, 6781.
5. Yokoma, Y.; Ricco, T. J Appl Polym Sci 1997, 66, 1007.
6. Karger-Kocsis, J. Polypropylene—Structure, Blends and Composites; Chapman & Hall: London, 1994.
7. Qiu, G. X.; Raue, F.; Ehrenstein, G. W. J Appl Polym Sci 2002, 83, 3029.
8. Pillow, J. G. Kautsch Gummi Kunstst 1998, 51, 855.
9. Sylvest, R. T.; Lancester, G.; Betso, S. R. Kautsch Gummi Kunstst 1997, 50, 186.
10. Raue, F.; Ehrenstein, G. W. J Elast Plast 1999, 31, 194.
11. Campbell, D.; White, J. R. Polymer Characterization; Chapman & Hall: New York, 1989.
12. Shieh, Y. T.; Lee, M. S.; Chen, S. A. Polymer 2001, 42, 4439.
13. Ha, C. S.; Kim, S. C. J Appl Polym Sci 1988, 35, 2211.
14. Park, J. Y.; Kwon, M. H.; Park, O. O. J Polym Sci Part B: Polym Phys 2000, 38, 3001.
15. Kirshenbaum, I.; Wilchinsky, Z. W.; Groten, B. J Appl Polym Sci 1964, 8, 2723.
16. Alamo, R. G.; Graessley, W. W.; Krishnamoorti, R.; Lohse, D. J.; Londono, J. D.; Mandelkern, L.; Stehling, F. C.; Wignall, G. D. Macromolecules 1997, 30, 561.
17. Herrero, C. H.; Acosta, J. L. Polymer 1994, 26, 786.
18. De Juana, R.; Jauregui, A.; Calahora, E.; Cortazar, M. Polymer 1996, 37, 3339.
19. Lee, S. W.; Ree, M.; Park, C. E.; Jung, Y. K.; Park, C. S.; Jin, Y. S. Polymer 1999, 40, 7137.
20. Ozawa, T. Polymer 1971, 12, 150.
21. Ozawa, T. Polymer 1978, 19, 1142.
22. Ziabicki, A. Colloid Polym Sci 1974, 6, 252.
23. Ziabicki, A. Appl Polym Symp 1967, 6, 1.
24. Liu, T. X.; Mo, Z. S.; Wang, S. E.; Zhang, H. F. Polym Eng Sci 1997, 37, 568.
25. Caze, C.; Devaux, E.; Crespy, A.; Cavrot, J. P. Polymer 1997, 38, 497.
26. Nakamura, K.; Katayama, K.; Amano, T. J Appl Polym Sci 1973, 17, 1031.
27. Chan, T. W.; Isayev, A. I. Polym Eng Sci 1994, 34, 461.
28. Avrami, M. J Chem Phys 1939, 7, 1103.
29. Avrami, M. J Chem Phys 1940, 8, 212.
30. Jeziorny, A. Polymer 1978, 19, 1142.
31. Tobin, M. C. J Polym Sci Polym Phys Ed 1974, 12, 399.
32. Seo, Y. S.; Kim, J. H.; Kin, K. U.; Kim, Y. C. Polymer 2000, 41, 2639.
33. Xu, W. B.; Ge, M. L.; He, P. S. J Appl Polym Sci 2001, 82, 2281.
34. Xu, W. B.; Ge, M. L.; He, P. S. Acta Polym Sinica 2001, No. 5, 584.
35. Kissinger, H. E. J Res Natl Bur Stand 1956, 57, 217.
36. Jang, G. S.; Cho, W. J.; Ha, C. S. J Polym Sci Part B: Polym Phys 2001, 39, 1001.
37. Lovinger, A. J.; Chua, J. O.; Gryte, C. C. J Polym Sci Polym Phys Ed 1977, 15, 64.
38. Guan, Y.; Wang, S. Z.; Zheng, A. N.; Xiao, H. N. J Appl Polym Sci 2003, 88, 872.